HHS Public Access

Author manuscript

Leukemia. Author manuscript; available in PMC 2023 April 08.

Published in final edited form as:

Leukemia. 2023 April ; 37(4): 728–740. doi:10.1038/s41375-023-01853-9.

KDM6B protects T-ALL cells from NOTCH1-induced oncogenic stress

Nancy Issa[1], **Hassan Bjeije**[1], **Elisabeth R. Wilson**[1], **Aishwarya Krishnan**[1], **Wangisa M.B. Dunuwille**[1], **Tyler M. Parsons**[1], **Christine R. Zhang**[1], **Wentao Han**[1], **Andrew L. Young**[1], **Zhizhong Ren**[2], **Kai Ge**[2], **Eunice S. Wang**[3], **Andrew P. Weng**[4], **Amanda Cashen**[1], **David H. Spencer**[1], **Grant A. Challen**[1,^]

[1]Division of Oncology, Department of Medicine, Washington University School of Medicine, St. Louis, MO, USA, 63110.

[2]National Institute of Diabetes and Digestive and Kidney Diseases, National Institutes of Health, Bethesda, MD 20892

[3]Roswell Park Comprehensive Cancer Center, Buffalo, NY 14263

[4]Terry Fox Laboratory, BC Cancer Agency, Vancouver, BC, Canada

Abstract

T-cell acute lymphoblastic leukemia (T-ALL) is an aggressive hematopoietic neoplasm resulting from the malignant transformation of T-cell progenitors. While activating *NOTCH1* mutations are the dominant genetic drivers of T-ALL, epigenetic dysfunction plays a central role in the pathology of T-ALL and can provide alternative mechanisms to oncogenesis in lieu of or in combination with genetic mutations. The histone demethylase enzyme *KDM6A* (*UTX*) is also recurrently mutated in T-ALL patients and functions as a tumor suppressor. However, its gene paralog, *KDM6B* (*JMJD3*), is never mutated and can be significantly overexpressed, suggesting it may be necessary for sustaining the disease. Here, we used mouse and human T-ALL models to show that *KDM6B* is required for T-ALL development and maintenance. Using *NOTCH1* gain-of-function retroviral models, mouse cells genetically deficient for *Kdm6b* were unable to propagate T-ALL. Inactivating *KDM6B* in human T-ALL patient cells by CRISPR/Cas9 showed *KDM6B*-targeted cells were significantly outcompeted over time. The dependence of T-ALL cells on *KDM6B* was proportional to the oncogenic strength of *NOTCH1* mutation, with KDM6B required to prevent stress-induced apoptosis from strong NOTCH1 signaling. These studies

^Co-corresponding author: Grant A. Challen, Ph.D., Washington University School of Medicine, 660 Euclid Avenue, St. Louis, MO, USA, 63110, Ph: +1 314-362-0987, grantchallen@wustl.edu.

AUTHOR CONTRIBUTIONS

Conceptualization and study design – G.A.C.
Experimentation and data acquisition – N.I, H.B., A.K., W.M.B.D., T.M.P, C.R.Z., W.H., G.A.C.
Data analysis – N.I., E.R.W., A.L.Y., D.H.S., G.A.C.
Resources and reagents – Z.R., K.G., E.S.W., A.P.W., A.C.
Funding acquisition – G.A.C.
Project administration and supervision – G.A.C.
Manuscript preparation – G.A.C.

DECLARATION OF INTERESTS

G.A.C. has performed consulting and received research support from Incyte (unrelated to this work). The remaining authors have declared that no conflict of interest exists.

identify a crucial role for *KDM6B* in sustaining *NOTCH1*-driven T-ALL and implicate KDM6B as a novel therapeutic target in these patients.

INTRODUCTION

The genomics era has facilitated remarkable advances in understanding the mechanisms driving the biology and pathogenesis of many blood cancers such as acute lymphoblastic leukemia (ALL). T-cell ALL (T-ALL) accounts for approximately 15% of pediatric and 25% of adult ALL cases respectively. Compared to the more common B-cell ALL, adult T-ALL cases are historically linked with a poor prognosis (1), due to unfavorable clinical features such as high white blood cell count, bulky adenopathy and central nervous system (CNS) involvement (2). While the advent of high-dose, multi-agent chemotherapy regimens have resulted in long-term event-free survival (EFS) rates of up to 90% in pediatric T-ALL, this clinical benefit has not carried over to the adult T-ALL patient population which have 5-year EFS rates of 40–50%. Clinical outcomes of patients with primary resistant or relapsed leukemia remains poor, and adult T-ALL patients remain at increased risk for induction failure and early relapse (3, 4). The differences in treatment outcomes are likely related to underlying genetic differences between children and adults. More specific therapies are needed for high-risk adult T-ALL patients based on their genetic profile.

T-ALL arises from the accumulation of genomic abnormalities that induce aberrant proliferation, increased cell survival, and impaired differentiation of immature T-cell progenitors. In the past decade, sequencing approaches have identified more than 100 genes mutated in T-ALL patient genomes (5), with *NOTCH1* gain-of-function variants being the most common oncogenic drivers (6). However, efforts to target NOTCH1 have had limited success due to major off-target toxicities (7). Studies have also revealed a high frequency of mutations in epigenetic regulators in T-ALL patients (8), with approximately 35% of adult T-ALL cases harboring a mutation in some component of the epigenetic machinery (9). This includes frequent mutations in components (e.g. *EZH2*, *SUZ12*, *JARID2*) of the polycomb repressive 2 (PRC2) complex which establishes the repressive epigenetic mark of H3K27me3 (10, 11). The gene encoding the histone lysine demethylase *KDM6A*, which catalyzes removal of H3K27me3, is also recurrently mutated in these patients and is thought to function as a cell-type and context-dependent tumor suppressor in this disease (12). Conversely, its gene paralog *KDM6B*, also known as *JMJD3*, is never mutated in T-ALL (13), but rather is often overexpressed in these patients (12) and other hematological disorders (14, 15). This dichotomy presented the hypothesis that while KDM6A may function as a tumor suppressor in T-ALL, KDM6B may actually be necessary for leukemic cell function in this blood cancer.

In a previous study, we demonstrated with mouse models that *Kdm6b* was necessary for leukemia development in certain contexts (16). Here, we show *KDM6B* is required for T-ALL maintenance using mouse and human genetic models. Utilizing a knockin mouse model harbouring point mutations in Kdm6b that abolish its catalytic activity confirmed that the pro-tumorigenic role of Kdm6b in T-ALL was largely related to its molecular function as a histone demethylase enzyme. Analysis of human T-ALL patient specimens

determined that the genetic dependence of these cells on *KDM6B* was directly related to the signal strength of different *NOTCH1* mutations, with the patients with most robust NOTCH1 signaling being most dependent on KDM6B. KDM6B was required to protect these cells from stress-induced apoptosis, a finding corroborated in mouse models using a "weak" *Notch1* mutation which indicated no reliance on *Kdm6b* for T-ALL cell function in this mutational background. Cumulatively, these studies reveal a novel role for *KDM6B* as a genetic dependency in T-ALL driven by strong *NOTCH1* gain-of-function mutations and highlight a new therapeutic target for this patient population.

METHODS

Mice and Transplantation

C57Bl/6 *Kdm6b*$^{fl/fl}$ (17) mice were crossed to Vav-Cre (18) or Mx1-Cre (19) strains. Six doses (300 μg/ mouse) of polyinosinic:polycytidylic acid (pIpC; Sigma #p1530) were administered every other day via intraperitoneal injection to induce Mx1-Cre. *Kdm6b*$^{H1388A/E1390A}$ catalytic dead knockin mice were previously described (20). For mouse bone marrow transplantation, recipient C57Bl/6 CD45.1 mice (The Jackson Laboratory #002014) were transplanted by retro-orbital injection following a split dose (~4 hours apart) of lethal irradiation (11 Gy). Patient-derived xenograft (PDX) models were generated by transplanting primary T-ALL patient cells into 6–8 week-old NOD-*scid* IL2Rgamma^{null} (NSG; The Jackson Laboratory #005557) via tail vein injection in a volume of 200 μL with 27-gauge U-100 insulin syringes (Easy Touch # 08496-2755-01).

Human T-ALL Samples

De-identified bone marrow samples were obtained from T-ALL patients and cultured *in vitro* in StemSpan SFEM II Media (StemCell Technologies #09655) supplemented with Pen-Strep (50 Units/mL), human stem cell factor (SCF; 50 ng/mL), human IL-2 (50U/mL), and human IL-7 (10 ng/mL).

Flow Cytometry

All antibody staining was performed in HBSS buffer (Corning #21021CV) containing Pen/Strep (100 Units/mL; Fisher Scientific #MT30002CI), HEPES (10uM; Life Technologies #15630080) and SerumPlus II Medium Supplement (2%; Sigma #14009C). Bone marrow cells isolated from tibias, femurs, and iliac crests were combined for calculating total BM from each mouse. Peripheral blood, bone marrow, and spleen cells were suspended in complete HBSS (1.0×10^8 cells/mL) and incubated on ice for >20 minutes with the following antibodies as needed (all 1:100 dilution): anti-mouse CD45.2-BV421 (BioLegend #109831), anti-mouse Ly-6A/E (Sca-1)-APC (BioLegend # 122512), anti-mouse c-Kit-BV421 (BioLegend #105828), anti-mouse CD25-PE (BD Biosciences #553866), anti-mouse CD3e-APCcy7 (BioLegend #100330), anti-mouse CD4-APC (BioLegend #100515), anti-mouse CD8-PEcy7 (BD Biosciences #552877), anti-human CD45-APC (BioLegend #368512), anti-human CD7-FITC (BioLegend #343104).

Plasmids and Viral Transduction

293T cells (ATCC #CRL-3216) were co-transfected with packaging vector (pCL-Eco) and either empty vector control MSCV-IRES-GFP (MIG), MIG-NICD, or MIG-NOTCH1-L1601P-ΔPEST using polyethylenimine (PEI; ThermoFisher Scientific #NC1014320). Viral supernatant was collected 48-hours post-transfection and centrifuged for 10 minutes to remove cell debris. Retrovirus-containing supernatant was aliquoted and frozen at −80°C. For retroviral transduction, mice were injected with 5-flurouracil (150 mg/kg) 6-days prior to experimentation. Bone marrow was collected and Sca-1+ cells were purified using magnetic selection (Miltenyi Biotec). 1.0×10^6 Sca-1+ BM cells / 500 μL were plated in Stempro-34 medium (Gibco #10639011) supplemented with Pen/Strep (100 units/mL), L-glutamine (2 mM), mSCF (100 ng/mL), mTPO (100 ng/mL), mFlt3L (50 ng/ mL), mIL-3 (5 ng/mL), and polybrene (4 μg/mL; Sigma), and spinfected with retrovirus supernatant at 250 g for 2 hours. Media was refreshed six hours post-transduction, and cells were collected 24 hours post-transduction for cell sorting and transplantation.

Western Blot

Cells were washed twice with PBS, sonicated for 5 minutes, and the cell lysates were loaded on SDS-PAGE gels, transferred to polyvinylidene fluoride membranes (Fisher Scientific, IPVH00010), and blocked with 5% non-fat milk in Tris-buffered saline with 0.1% Tween 20 detergent (TBST). The blots were incubated with the indicated primary antibodies at 4°C overnight. Western blots were probed with antibodies to detect NICD (Cell signaling, #4147S) and β-ACTIN (Santa Cruz, SC-47778). The next day, the blots were washed with TBST and incubated with the suitable mouse or rabbit secondary antibody (Fisher Scientific, 55965-84-9, 10794347) at room temperature for one hour. Detection was performed using horseradish peroxidase conjugated secondary mouse or rabbit antibody and chemiluminescence HRP substrate (Millipore #WBKLS0100). The blots were then visualized on a Bio-Rad ChemiDOC Touch Imaging System (Bio-Rad Laboratories).

RNA-Seq

RNA was isolated using the NucleoSpin RNA XS kit (Macherey-Nagel #740902.250). The SMARTer Ultra Low RNA kit (Clontech) was used to prepare libraries for RNA-seq as per manufacturer instructions. Sequencing was performed with an Illumina NovaSeq S4 2×150. Analysis was performed using Partek flow software. Raw RNA-seq reads were aligned to the Ensembl release 99 (Mouse), and to the Ensembl release 105 (Human) using STAR version 2.7.3a. Quality control was performed to confirm the efficacy of the alignment and the quality of the reads. Gene counts were normalized and Gene Specific Analysis (GSA) was performed on the normalized counts to generate the differential analysis. Gene set enrichment analysis (GSEA) was generated to identify dysregulated gene sets. Primary data is available under GEO accession number GSE214576.

CRISPR/Cas9 and Targeted Deep Sequencing

Synthetic guide RNAs (gRNAs) were designed using the UCSC Genome browser software. gRNAs were selected to target the catalytic domain of KDM6B to maximize specificity (lowest off-target effects) and efficiency (on-target cleavage efficiency)(21). The four highest

scoring gRNAs were tested by nucleofecting HEL cells. 48-hours post-nucleofection, DNA was extracted from cells in each group and sent for next generation sequencing (NGS). The two gRNAs with the highest targeting efficiency were used for experimentation. Primary human T-ALL cells were nucleofected with Cas9/ribonucleoprotein (IDT, #1074181) complexed with gRNAs as previously described (37). Synthetic gRNAs (Synthego) sequences are as follows: KDM6B_18a: TGCTCCGTCAACATCAACAT, KDM6B_18d: CGCGGTGCACGAGCACTACT. A gRNA targeting the AAVS1 locus was used as a negative control: GGGGCCACUAGGGACAGGAU. Post-nucleofection, cells were left to recover in StemSpan SFEM II Media (StemCell Technologies #09655) supplemented with Pen-Strep (50 Units/mL), human stem cell factor (SCF; 50 ng/mL), human IL-2 (50U/mL), and human IL-7 (10 ng/mL). 48-hours later, approximately 100,000 cells were set aside to measure targeted variant allele fraction (VAF) using PCR amplicon-based deep sequencing. The remaining cells were transplanted into NSG mice via tail vein injections, where each mouse received 250,000 nucleofected cells. Serial monthly bleeds were performed where CD45+ CD7+ human T-ALL cells were purified, DNA was extracted using the PureLink Genomic DNA Mini Kit (Thermo Fisher Scientific, # K1820-02), and VAF was monitored over time. The following primer pairs were used to generate amplicons: AAVS1_Forward – ACAGGAGGTGGGGGTTAGAC plus AAVS1_Reverse – CCCCTATGTCCACTTCA; KDM6B_18_Forward – CAGCCAATGAGGGCAGAG plus KDM6B_18_Reverse - CACAGGTCAGGTGGGAACTG. Amplicon-based deep-sequencing libraries were sequenced using the Illumina MiSeq platform and data analyzed using CRISPResso2 (22).

AnnexinV Staining

Cells were stained with antibodies to identify T-ALL cells (mouse: CD45.2+ GFP+; human: hCD45+ CD7+), then washed twice with cold PBS and incubated at room temperature for 15 minutes in 1x AnnexinV binding buffer (Fisher, # 50-927-9) containing AnnexinV–APC (Fisher, # 50-927-9) and Sytox blue cell stain (Fisher, # 501137613). Cells were analyzed by flow cytometry within one hour of staining.

Ki67 Cell Cycle Assay

Cells were stained with antibodies to identify T-ALL cells (mouse: CD45.2+ GFP+; human: hCD45+ CD7+), then washed twice with cold PBS. The cell pellet was loosened by vortexing and three mL of cold 70% ethanol was added dropwise to the cell pellet while vortexing. Samples were incubated with the 70% ethanol at −20°C for one hour. After fixation, samples were washed three times with the Cell Staining Buffer (BioLegend, # 420201) then stained with fluorochrome-conjugated Ki67 antibody (BioLegend, # 652413) at 1:100 dilution at the concentration of 1.0×10^6 / mL. Samples were incubated in the dark for 30 minutes, then washed twice with Cell Staining Buffer, and resuspended in 0.5 mL cell staining buffer for flow cytometric analysis.

Statistics

Student t-test, one-way, and two-way ANOVA were used for statistical comparisons where appropriate. Survival curves were analyzed using a Mantel-Cox logrank test. Significance

is indicated using the following convention: *p<0.05, **p<0.01, ***p<0.001,****p<0.0001. All graphs represent mean ± S.E.M.

Study Approval

All animal procedures were approved by the Institutional Animal Care and Use Committee at Washington University. Human T-ALL patient samples were obtained with written consent in accordance with the Declaration of Helsinki protocol. Because all patient samples were de-identified and the study team had no access to individual patient health information (PHI), the Washington University Institutional Review Board (IRB) and Human Research Protection Office (HRPO) determined this to be a non-human study.

RESULTS

Kdm6b is essential for maintenance of NOTCH1-mutant T-ALL cells

A retroviral model of NOTCH1 intracellular domain (NICD) expression that recapitulates many of the human pathologies of *NOTCH1*-mutant T-ALL (23) was used to examine the role of *Kdm6b* in T-ALL development. A conditional knockout model was generated by crossing the Vav-Cre driver (18) to delete floxed exons 14–20 of *Kdm6b* (17) in hematopoietic cells. Sca-1-enriched bone marrow (BM) from Vav-Cre:$Kdm6b^{+/+}$ (Control), Vav-Cre:$Kdm6b^{fl/+}$ (HET), and Vav-Cre:$Kdm6b^{fl/fl}$ (KO) adult mice was transduced with a GFP-containing retrovirus expressing NICD (MIG-NICD). 500 transduced BM progenitor cells (GFP+ Lineage-c-Kit+ Sca-1+) were purified and transplanted with a radioprotective dose of 3.0×10^5 congenic (CD45.1) BM cells into lethally CD45.1 irradiated mice. There was robust engraftment of T-ALL cells from all groups four-weeks post-transplant (Figure 1A), and the immunophenotype of engrafted T-ALL cells was similar amongst genotypes (Supplemental Figure 1). Mice receiving NICD-GFP+ cells with either wild-type or heterozygous *Kdm6b* succumbed to T-ALL with similar latency (median survival = 76 and 79 days respectively; Figure 1B). However, despite no evidence of engraftment defects four-weeks post-transplant, mice receiving *Kdm6b*-KO NICD-GFP+ cells did not propagate T-ALL within the observation period (Figure 1B) with no evidence of residual T-ALL in the BM (Figure 1C). Serial analysis of the peripheral blood showed T-ALL cells were not sustained in the absence of *Kdm6b* (Figure 1D). Analysis of moribund control and *Kdm6b*-HET mice displayed significant T-ALL cell burden in all hematopoietic organs. Mice that received the *Kdm6b*-KO cells showed no evidence of T-ALL in the BM (Figure 1C) and spleen (Figure 1E–G) at the time of sacrifice. These data suggested *NOTCH1*-mutant T-ALL cells require some level of Kdm6b for their propagation.

To circumvent any potential complications of initial T-ALL cell engraftment, an analogous experiment was performed using cells from inducible Mx1-Cre:$Kdm6b^{fl/fl}$ mice. NICD-GFP transduced Sca-1+ BM cells were transplanted and then deletion of *Kdm6b* was induced 5-weeks post-transplant when engraftment levels were comparable (Supplemental Figure 2A). Following injection of pIpC, there was no difference in overall survival between recipients of Mx1-Cre:$Kdm6b^{fl/fl}$ and Mx1-Cre:$Kdm6b^{+/+}$ (control) T-ALL cells (Supplemental Figure 2B). However, while injection of pIpC was relatively efficient at inducing Mx1-Cre and recombination of floxed alleles in Mx1-Cre:$Kdm6b^{fl/fl}$ T-ALL cells

one-week post-treatment, the cells that underwent recombination were rapidly outcompeted by three-weeks post-treatment (Supplemental Figure 2C). Thus, the observed survival outcome of Mx1-Cre:*Kdm6b*$^{fl/fl}$ recipients was likely due to T-ALL cells that escaped recombination rapidly outcompeting cells successfully induced for *Kdm6b* deletion. This is an indirect indication that *Kdm6b* is necessary for maintenance of *NOTCH1*-mutant T-ALL cells.

T-ALL cells undergo apoptosis in the absence of Kdm6b

To begin to understand the molecular mechanism of functional dependence for *NOTCH1*-mutant T-ALL cells on *Kdm6b*, gene expression analysis was performed by RNA-seq on T-ALL cells (CD45.2+ NICD-GFP+) isolated from the blood of recipient mice four-weeks post-transplant. Comparison of gene expression profiles of control and *Kdm6b*-KO (Supplemental Table 1) identified 210 differentially expressed genes (>2-fold change, $p<0.05$, FDR <0.05). The majority of these genes showed decreased expression in *Kdm6b*-KO T-ALL cells (Figure 2A). Gene set enrichment analysis (GSEA) identified three significantly differential pathways – “E2F targets”, “G2M checkpoint”, and “mitotic spindle”, all of which were downregulated in *Kdm6b*-KO T-ALL cells (Figure 2B). Given this, we hypothesize that Kdm6b may be necessary for cell cycle progression of T-ALL cells. To examine this, Ki67 cell cycle assay was performed on T-ALL cells from peripheral blood of recipient mice at four-weeks post-transplant (Figure 2C). *Kdm6b*-KO T-ALL cells showed a slight yet significant decrease in the proportion of cells in the G_2/M phase of cell cycle (Figure 2D). While this was suggestive of a slight cell cycle arrest of *Kdm6b*-KO T-ALL cells, it appeared unlikely that this relatively minor difference could account for the large discrepancy in T-ALL cell maintenance. To determine if the cell cycle differences had any impact on cell survival, apoptosis analysis was performed on T-ALL cells by AnnexinV staining (Figure 2E). There was a striking increase in T-ALL cell apoptosis in the absence of *Kdm6b* (Figure 2F). This suggests that the primary function of Kdm6b in *NOTCH1*-mutant T-ALL cells may be to prevent leukemia cell apoptosis.

Pro-tumorigenic function of Kdmb6 in T-ALL is demethylase-dependent

KDM6B is described to function primarily as a H3K27me3 histone demethylase enzyme (24, 25), yet recent studies have suggested that KDM6B may have other demethylase-independent activities (13, 26, 27). To determine if the function of Kdm6b in T-ALL was dependent on histone demethylase function, a mouse model was utilized with two engineered point mutations in the same germline allele of Kdm6b (*Kdm6b*$^{H1388A;H1390A}$) that abolish the catalytic activity of the protein (24, 28). As homozygous *Kdm6b*$^{H1388A;H1390A}$ mice are embryonic lethal (Dr. Kai Ge, unpublished data), we crossed *Kdm6b*$^{H1388A;H1390A/+}$ mice to Vav-Cre:*Kdm6b*$^{fl/fl}$ mice to generate Vav-Cre:*Kdm6b*$^{fl/H1388A;H1390A}$ such that the only copy of *Kdm6b* expressed in hematopoietic cells is catalytically dead (CD). The NICD retroviral transduction and transplantation model was repeated to include this genotype. The significant difference in survival of recipient mice transplanted with NICD-GFP expressing *Kdm6b*-HET and *Kdm6b*-KO cells allowed evaluation of the catalytic function of Kdm6b in this activity. If survival of mice receiving NICD-GFP expressing *Kdm6b*-CD cells resembled that of *Kdm6b*-KO cells, then the function of Kdm6b in T-ALL is demethylase-dependent. However, if the survival of these

mice mirrored that of NICD-GFP expressing *Kdm6b*-HET cells, this suggests the function of Kdm6b in T-ALL is histone demethylase-independent. Despite comparable levels of initial engraftment, analysis of recipient mice eight-weeks post-transplant revealed a dearth of *Kdm6b*-CD T-ALL cells in the peripheral blood (Figure 3A). T-ALL cells were unable to propagate in a *Kdm6b*-CD genetic background, replicating the overall survival of mice receiving *Kdm6b*-KO cells (Figure 3B). The few mice that developed *Kdm6b*-KO and *Kdm6b*-CD T-ALL in these experiments were found to have retained one copy of the wild-type *Kdm6b* allele (functionally a *Kdm6b*-HET). These results strongly suggest that the function of Kdm6b in sustaining *NOTCH1*-mutant T-ALL cells is demethylase-dependent.

KDM6B is required to sustain disease in a subset of T-ALL patients

To investigate the translational potential of our findings, *KDM6B* was inactivated in primary human patient T-ALL cells by CRISPR/Cas9 gene targeting. Four guide RNAs (gRNAs) were designed to target the exons encoding the catalytic domain of *KDM6B* (29). The two gRNAs that showed the highest targeting efficiency in HEL cells were used for experimentation. A gRNA that targets the inert *AAVS1* locus was used as a negative control. For genetic consistency, only *NOTCH1*-mutant T-ALL patient samples were used in these experiments (Table 1). gRNA/Cas9 ribonucleoprotein (RNP) complexes (30) were nucleofected into primary human T-ALL cells and 48-hours post-nucleofection, 2.5×10^5 nucleofected cells were xenografted into three NSG mice per gRNA per patient, with the remaining T-ALL cells processed for genomic DNA extraction to quantify initial CRISPR targeting efficiency by amplicon-based deep sequencing. In general, no significant differences were noted between the *AAVS1* and *KDM6B* gRNA groups across different patient samples as assessed by monthly analysis of the peripheral blood, time to morbidity, or leukemic burden in the BM and spleen of moribund mice. However, analysis of the variant allele fraction (VAF) of CRISPR targeted cells over time revealed a striking trend and segregated the response of patient cells into two distinct entities. For 3/8 adult T-ALLs, the VAF of the edited *KDM6B* alleles remained relatively constant over time, suggesting that these specific patient samples were insensitive to genetic loss of *KDM6B* (Figure 4A, Supplemental Figure 3A; “non-responders”). In contrast, 5/8 T-ALL samples showed a marked reduction in *KDM6B* VAF over time, showing the edited cells were rapidly outcompeted *in vivo* (Figure 4B, Supplemental Figure 3B). Patient samples that showed >50% decrease in VAF of *KDM6B* at the conclusion of the transplant compared to the input were termed “responders”. Analysis of VAF over the experimental timecourse showed that in most specimens, the VAF of control *AAVS1* edited alleles remained relatively consistent (Figure 4C). However, similar comparison of the VAF of *KDM6B* edited alleles showed that while the targeted cells were efficiently retained in the non-responder patient specimens, the targeted cells were rapidly outcompeted over time in the responder T-ALL patient cells (Figure 4C).

While the focus of these translational studies was adult T-ALL samples due to the inferior clinical outcomes of this demographic, we also performed analogous CRISPR/Cas9 experiments with a limited set of *NOTCH1*-mutant pediatric T-ALL primary specimens. Of the three samples tested, one classified as a non-responder (Supplemental Figure 4A) whereas two acted as responders with rapid depletion of *KDM6B* targeted cells

(Supplemental Figure 4B). This was reinforced by dynamic comparisons of *AAVS1* versus *KDM6B* VAFs over the experimental timecourse (Supplemental Figure 4C). Cumulatively, these experiments with primary T-ALL patient samples suggests that as in mouse models, *KDM6B* was required for the efficient propagation of T-ALL cells, but only for a specific subset of patients.

We sought to determine if genetic dependency on *KDM6B* in T-ALL patients correlated with clinical outcomes. For the three pediatric specimens subject to functional analysis, all of the patients survived their T-ALL. The two *KDM6B* "responder" pediatric patients achieved durable complete remission (CR) after induction chemotherapy, whereas the *KDM6B* "non-responder" suffered CNS relapse after initial response, but underwent successful allogeneic stem cell transplantation. Only one of the eight adult T-ALL patients surveyed in this study survived their disease (a *KDM6B* "responder"). Due to the complex treatment histories and transplant complications, it was not possible to correlate clinical outcomes with *KDM6B* reliance in this relatively small patient cohort.

KDM6B restrains expression of pro-apoptotic genes in KDM6B-dependent T-ALLs

To explore potential clinical application of KDM6B inhibition, the small molecule GSK-J4 has been proposed as a H3K27 histone demethylase family inhibitor that has evidence of effectiveness in T-ALL (12). We exposed two "responder" and two "non-responder" patient samples to increasing concentrations of GSK-J4 but did not note any differences in sensitivity (Figure 5A). Moreover, the sensitivity was not affected by CRISPR-mediated *KDM6B* gene deletion (Figure 5B). Thus, GSK-J4 does not appear to be specific enough for KDM6B inhibition in T-ALL, and any benefit may be due to inhibition of KDM6A or other off-target effects on α-ketoglutarate-dependent enzymes (31).

To begin to elucidate the mechanisms of KDM6B dependence in human patient samples, adult "responder" and "non-responder" T-ALL specimens were targeted with *AAVS1* and *KDM6B* gRNAs and cultured *in vitro* for seven days. Due to the rapid depletion of *KDM6B*-targeted cells *in vivo*, this approach was taken to study molecular profiles of *KDM6B*-inhibited T-ALL while the tumor still contained a high fraction of edited cells. Global transcriptomic analysis was performed after confirming high targeting efficiency of the edited cells (Figure 5C). Unsupervised clustering of RNA-seq data showed that samples grouped more strongly by individual patient heterogeneity rather than dependence on *KDM6B* (Figure 5D). Due to this, further analysis was performed to aggregate responder versus non-responder samples under control conditions (*AAVS1* gRNA) compared KDM6B inhibition (*KDM6B* gRNA). Under control conditions, only 216 genes were differentially expressed between responders and non-responders (>2-fold expression difference, p-value <0.05). However, following *KDM6B* targeting, 1229 genes became significantly differentially expressed (Supplemental Table 2). GSEA of the two specimen groups under control conditions revealed many of the same pathways identified in mouse RNA-seq such as "E2F targets" and "G2M checkpoint" (Figure 5E). However, GSEA of the *KDM6B* targeted cells (Figure 5F) revealed specific enrichment of "apoptosis" pathway genes (Figure 5G) that was not observed in the *AAVS1*-targeted cell comparison. Thus, KDM6B appears necessary for preventing apoptosis in a subset of *NOTCH1*-mutant

human T-ALL patients, corroborating previous findings in mouse models. To analyze this further, AnnexinV staining was performed on T-ALL patient specimens cultured *in vitro* for seven days following CRISPR with either *AAVS1* or *KDM6B* gRNAs. While some responder patients showed a subtle yet significant increase in the proportion of apoptotic cells following targeting with *KDM6B* (Figure 5H), in general this genetic manipulation was insufficient to induce robust T-ALL cell death (Figure 5I). This is likely due to complicating factors such as variable CRISPR targeting efficiency, cell culture conditions optimized to maintain viability of T-ALL cells, and the lack of cell competition / selective pressures of an *in vivo* experiment.

Genetic signature of KDM6B dependence in T-ALL

We attempted to integrate transcriptome and mutation profile to identify why only a subset of T-ALL patient specimens were sensitive to *KDM6B* inhibition. Expression levels of *KDM6B* itself or the paralog *KDM6A* were not different between adult responders and non-responders (Figure 6A). Exome sequencing data of human T-ALL patient samples was examined to determine if the dependence on KDM6B for certain specimens correlated with the type of *NOTCH1* mutation or the nature of co-operating mutations. The VAF of *NOTCH1* mutations in the primary tumor samples was not different between responders and non-responders (Figure 6B). Analysis of the mutational distribution mutations showed that the *NOTCH1* mutations found in non-responders were all localized between amino acids 1585-1593 in the N-terminus of the heterodimerization (HD) domain (Figure 6C). Mutations in the *NOTCH1* HD domain act as gain-of-function by inducing ligand-independent activation of the receptor (32, 33), but the mutation pattern was not significantly different between responders and non-responders (Figure 6C). With regard to cooperating mutations, the sample size precluded generation of definitive conclusions, however, some patterns of mutational cooperation emerged (Figure 6D). Patients in the responder group were more likely to have multiple *NOTCH1* mutations with 2/7 patients having >1 *NOTCH1* mutation (Figure 6E) compared to 0/4 in the non-responder group. Additionally, *FBXW7* mutations were identified in 2/7 responder patients (mutually exclusive of responder patients with multiple *NOTCH1* mutations) compared to 0/4 non-responder patients with *FBXW7* mutations (Figure 6D). FBXW7 is a ubiquitin ligase that negatively regulates stability of NICD. Mutations in *FBXW7* occur in ~15% of T-ALL patients (34, 35) which abrogate binding to NICD, thereby prolonging its half-life and potentiating NOTCH1 signaling. Both mutational patterns observed in KDM6B responders (multiple *NOTCH1* mutations, *NOTCH1* plus *FBXW7* mutations) serve to increase the strength of NOTCH1 signaling in T-ALL cells.

KDM6B protects T-ALL cells from strong NOTCH1 signaling-induced apoptosis

Cancers must develop mechanisms of tolerating various infidelities of oncogene-induced cellular stress. This includes T-ALL where *NOTCH1* mutations hijack the cellular stress response machinery to facilitate transformation by a number of mechanisms including upregulation of the heat shock response pathway (36) and increased nucleotide biosynthesis to overcome metabolic stress (37). As KDM6B responders were enriched for genetic mutations that further amplified NOTCH1 signaling in T-ALL patients, we hypothesized

KDM6B may be required to protect T-ALL cells from strong *NOTCH1*-induced oncogenic stress.

To examine NOTCH1 signal strength in T-ALL patient cells, western blot was performed to observe stability of the cleaved NICD protein. NICD levels were markedly higher in responder patient samples compared to KDM6B non-responders (Figure 7A). However, protein stability of NICD does not appear to be influenced directly by KDM6B as NICD levels were comparable in patient samples following CRISPR/Cas9-mediated deletion of *KDM6B* (Figure 7B). Consistent with increased NICD stability, there was increased expression of NOTCH1 target genes in T-ALL (38) such as *CCND3*, *CDK4* and *CDK6* in human responder samples versus non-responder patients, and increased expression of classical NOTCH1 signaling genes such as *Hes1*, *Hey1* and *Dtx1* in mouse *Kdm6b*-KO T-ALL cells (Figure 7C). To investigate the hypothesis that KDM6B is only required to protect T-ALL cells faced with strong NOTCH1 signaling, we utilized a retroviral model expressing a T-ALL mutant form of the NOTCH1 receptor (*NOTCH1*^{L1601P}-ΔPEST (39)) that induces weaker NOTCH1 signaling than the NICD-expressing retrovirus used in earlier studies (Figure 7D). We performed the same retroviral transduction experiment on Sca-1-enriched WBM from adult control, *Kdm6b*-HET and *Kdm6b*-KO mice. Four-weeks post-transplant, AnnexinV staining was performed on peripheral blood T-ALL cells to examine apoptosis. In contrast to NICD-driven T-ALL which induced significant apoptosis in *Kdm6b*-KO cells (Figure 2F), there was no difference in apoptosis between the T-ALL genotypes expressing *NOTCH1*^{L1601P}-ΔPEST (Figure 7E). Consistent with the apoptosis data, long-term monitoring of these mice revealed that *NOTCH1*^{L1601P}-ΔPEST-driven T-ALL developed at the same incidence amongst all genotypes of donor cells (Figure 7F). Cumulatively, these data show that Kdm6b protects T-ALL cells from oncogene stress-induced apoptosis where potent *NOTCH1* activating mutations induce strong NOTCH1 signaling.

DISCUSSION

Technological advances in genome sequencing technology have allowed unparalleled resolution into the spectrum of mutations present in cancer genomes, and virtually all of the important genetic drivers of T-ALL have now been identified (10, 40–42). Resulting investments into generating genetic tools to model how these mutations contribute to leukemogenesis has generated mechanistic insight into transformation of malignant T-cells. Unfortunately, this has not necessarily translated into new therapeutic approaches. An alternative strategy to identifying new drug targets in T-ALL is to define leukemia-essential genes, that is genes which are never mutated in a particular disease, indicating they may be essential for the survival and propagation of the malignant cells. Therapeutic inhibition of these gene products could thus potentially render the cells incompetent for malignant transformation. This study identifies *KDM6B* as an essential gene for *NOTCH1*-mutant T-ALL cells. Mouse hematopoietic progenitor cells deficient for *Kdm6b* were unable to initiate T-ALL driven by strong *NOTCH1* activating mutations, and primary T-ALL cells from human patients targeted for *KDM6B* loss-of-function by CRISPR/Cas9 gene editing were rapidly outcompeted by non-edited cells. These outcomes suggest *KDM6B* mutations

are never observed in T-ALL patients as this would result in loss of these clones due to competitive disadvantage.

For consideration of therapeutic targeting, we have previously shown that while genetic inhibition of *Kdm6b* leads to a competitive disadvantage of mouse hematopoietic stem and progenitor cells (HSPCs), this defect was only evident under stress conditions such as serial bone marrow transplantation or inflammation (16). Mice with complete absence of *Kdm6b* in the hematopoietic system are viable and show no overt phenotypes, suggesting inhibition of KDM6B (at least in the short term) can be tolerated by HSPCs and should no cause overt hematopoietic toxicity as a drug candidate. The small molecule GSK-J4 has been identified to inhibit KDM6B (31) and been shown to have efficacy against certain T-ALL cells *in vitro* (12). However, we show here that the activity of GSK-J4 against T-ALL cells was not dependent on KDM6B (Figure 5B). GSK-J4 is a catalytic site inhibitor of the JmjC domain conserved between KDM6B and KDM6A. Despite the high degree of sequence similarity between these proteins, recent studies have revealed surprisingly contrasting roles for these proteins in cellular reprogramming and cancer, including T-ALL where KDM6A functions as a gender-specific tumor suppressor (43). Thus, a more selective inhibitor that specifically targets KDM6B is necessary for translational applications. A more detailed understanding of the specific molecular functions by which KDM6B protects *NOTCH1*-mutant cells from apoptosis is required to achieve this. Our previous studies showed that the function of Kdm6b in normal hematopoiesis appears largely unrelated to chromatin regulation, as H3K27me3 patterns were not significantly different wild-type and *Kdm6b*-null HSPCs (16). In contrast, the protective function of Kdm6b in *NOTCH1*-mutant T-ALL was dependent on histone demethylase activity as catalytically-dead HSPCs were also unable to propagate T-ALL (Figure 3B). This justifies a screen for more specific enzymatic inhibitors of KDM6B as a therapy for *NOTCH1*-mutant T-ALL.

Translation of our findings from mouse models using primary patient samples identified a subgroup of *NOTCH1*-mutant T-ALL cells that were particularly sensitive to genetic inhibition of KDM6B. Although all primary samples used contained *NOTCH1* mutations for genetic consistency, there is considerable heterogeneity in the spectrum of *NOTCH1* variants within T-ALL patients (44). We found the “responder” patients had the highest level of NICD expression, conveying strong NOTCH1 signaling. Moreover, the “responder” group also contained the only patients with multiple *NOTCH1* mutations and patients which also carried *FBXW7* mutations which further amplify NOTCH1 signaling (35). We hypothesize that KDM6B is required in this subgroup of patients to protect the leukemia cells from NOTCH1 oncogene stress-induced apoptosis, although the precise mechanism of this protection conveyed by KDM6B remains to be determined in future studies. Cumulatively, this study identifies a novel role for KDM6B in maintenance of T-ALL driven by strong NOTCH1 signaling, which opens the possibility for a new class of therapeutic discovery for this subset of T-ALL patients.

Supplementary Material

Refer to Web version on PubMed Central for supplementary material.

ACKNOWLEDGEMENTS

We thank all members of the Challen laboratory for ongoing contributions and critical discussion. We thank the Alvin J. Siteman Cancer Center at Washington University School of Medicine and the Institute of Clinical and Translational Sciences (ICTS) at Washington for the use of the Tissue Procurement Core, which provided T-ALL patient samples. Support for procurement of human samples was provided by P50CA171963. The Siteman Cancer Center is supported in part by NCI Cancer Center Support Grant P30CA091842 and the ICTS is funded by the National Institutes of Health's NCATS Clinical and Translational Science Award (CTSA) program grant UL1TR002345. We thank the Roswell Park Hematological Procurement Shared Resource for T-ALL specimens which is supported by the NCI Cancer Center Support Grant 5P30CA001656. We thank the Siteman Cancer Center Flow Cytometry core, which is supported by NIH Cancer Center Support Grant P30CA091842. We thank the Genome Technology Access Center at the McDonnell Genome Institute at Washington University School of Medicine for genomic analyses. The Center is partially supported by NCI Cancer Center Support Grant P30CA91842. This publication is solely the responsibility of the authors and does not necessarily represent the official view of the NIH.

This work was supported by the National Institutes of Health (HL147978, CA236819 and DK124883 to G.A.C), Gabrielle's Angel Foundation (to G.A.C), Alex's Lemonade Stand Foundation (to G.A.C) and the Children's Discovery Institute (to G.A.C). C.R.Z. was supported by an American Society of Hematology post-doctoral scholar award and Edward P. Evans Center for MDS Post-Doctoral Fellowship. Z.R. and K.G. were supported by the Intramural Research Program of NIDDK, NIH. E.S.W. is supported by the Jacquie Hirsch Leukemia Research Fund. G.A.C. is a scholar of the Leukemia and Lymphoma Society.

DATA AVAILABILITY

Primary RNA-sequencing data are available through NCBI Gene Expression Omnibus under GEO accession number GSE214576.

REFERENCES

1. Pui CH, Robison LL, and Look AT. Acute lymphoblastic leukaemia. Lancet. 2008;371(9617):1030–43. [PubMed: 18358930]
2. Uckun FM, Gaynon PS, Sensel MG, Nachman J, Trigg ME, Steinherz PG, et al. Clinical features and treatment outcome of childhood T-lineage acute lymphoblastic leukemia according to the apparent maturational stage of T-lineage leukemic blasts: a Children's Cancer Group study. J Clin Oncol. 1997;15(6):2214–21. [PubMed: 9196133]
3. Goldberg JM, Silverman LB, Levy DE, Dalton VK, Gelber RD, Lehmann L, et al. Childhood T-cell acute lymphoblastic leukemia: the Dana-Farber Cancer Institute acute lymphoblastic leukemia consortium experience. J Clin Oncol. 2003;21(19):3616–22. [PubMed: 14512392]
4. Oudot C, Auclerc MF, Levy V, Porcher R, Piguet C, Perel Y, et al. Prognostic factors for leukemic induction failure in children with acute lymphoblastic leukemia and outcome after salvage therapy: the FRALLE 93 study. J Clin Oncol. 2008;26(9):1496–503. [PubMed: 18349402]
5. Girardi T, Vicente C, Cools J, and De Keersmaecker K. The genetics and molecular biology of T-ALL. Blood. 2017;129(9):1113–23. [PubMed: 28115373]
6. Belver L, and Ferrando A. The genetics and mechanisms of T cell acute lymphoblastic leukaemia. Nat Rev Cancer. 2016;16(8):494–507. [PubMed: 27451956]
7. Ferrando AA. The role of NOTCH1 signaling in T-ALL. Hematology Am Soc Hematol Educ Program. 2009:353–61. [PubMed: 20008221]
8. Huether R, Dong L, Chen X, Wu G, Parker M, Wei L, et al. The landscape of somatic mutations in epigenetic regulators across 1,000 paediatric cancer genomes. Nat Commun. 2014;5:3630. [PubMed: 24710217]
9. Neumann M, Vosberg S, Schlee C, Heesch S, Schwartz S, Gokbuget N, et al. Mutational spectrum of adult T-ALL. Oncotarget. 2015;6(5):2754–66. [PubMed: 25595890]
10. Zhang J, Ding L, Holmfeldt L, Wu G, Heatley SL, Payne-Turner D, et al. The genetic basis of early T-cell precursor acute lymphoblastic leukaemia. Nature. 2012;481(7380):157–63. [PubMed: 22237106]

11. Ntziachristos P, Tsirigos A, Van Vlierberghe P, Nedjic J, Trimarchi T, Flaherty MS, et al. Genetic inactivation of the polycomb repressive complex 2 in T cell acute lymphoblastic leukemia. Nat Med. 2012;18(2):298–301. [PubMed: 22237151]
12. Ntziachristos P, Tsirigos A, Welstead GG, Trimarchi T, Bakogianni S, Xu L, et al. Contrasting roles of histone 3 lysine 27 demethylases in acute lymphoblastic leukaemia. Nature. 2014.
13. Arcipowski KM, Martinez CA, and Ntziachristos P. Histone demethylases in physiology and cancer: a tale of two enzymes, JMJD3 and UTX. Curr Opin Genet Dev. 2016;36:59–67. [PubMed: 27151432]
14. Wei Y, Zheng H, Bao N, Jiang S, Bueso-Ramos CE, Khoury J, et al. KDM6B overexpression activates innate immune signaling and impairs hematopoiesis in mice. Blood Adv. 2018;2(19):2491–504. [PubMed: 30275007]
15. Ohguchi H, Harada T, Sagawa M, Kikuchi S, Tai YT, Richardson PG, et al. KDM6B modulates MAPK pathway mediating multiple myeloma cell growth and survival. Leukemia. 2017;31(12):2661–9. [PubMed: 28487543]
16. Mallaney C, Ostrander EL, Celik H, Kramer AC, Martens A, Kothari A, et al. Kdm6b regulates context-dependent hematopoietic stem cell self-renewal and leukemogenesis. Leukemia. 2019.
17. Iwamori N, Iwamori T, and Matzuk MM. H3K27 demethylase, JMJD3, regulates fragmentation of spermatogonial cysts. PLoS ONE. 2013;8(8):e72689. [PubMed: 23967333]
18. Georgiades P, Ogilvy S, Duval H, Licence DR, Charnock-Jones DS, Smith SK, et al. VavCre transgenic mice: a tool for mutagenesis in hematopoietic and endothelial lineages. Genesis. 2002;34(4):251–6. [PubMed: 12434335]
19. Kuhn R, Schwenk F, Aguet M, and Rajewsky K. Inducible Gene Targeting in Mice. Science. 1995;269(5229):1427–9. [PubMed: 7660125]
20. Nakka K, Hachmer S, Mokhtari Z, Kovac R, Bandukwala H, Bernard C, et al. JMJD3 activated hyaluronan synthesis drives muscle regeneration in an inflammatory environment. Science. 2022;377(6606):666–9. [PubMed: 35926054]
21. Doench JG, Fusi N, Sullender M, Hegde M, Vaimberg EW, Donovan KF, et al. Optimized sgRNA design to maximize activity and minimize off-target effects of CRISPR-Cas9. Nat Biotechnol. 2016;34(2):184–91. [PubMed: 26780180]
22. Clement K, Rees H, Canver MC, Gehrke JM, Farouni R, Hsu JY, et al. CRISPResso2 provides accurate and rapid genome editing sequence analysis. Nat Biotechnol. 2019;37(3):224–6. [PubMed: 30809026]
23. Pear WS, Aster JC, Scott ML, Hasserjian RP, Soffer B, Sklar J, et al. Exclusive development of T cell neoplasms in mice transplanted with bone marrow expressing activated Notch alleles. J Exp Med. 1996;183(5):2283–91. [PubMed: 8642337]
24. Xiang Y, Zhu Z, Han G, Lin H, Xu L, and Chen CD. JMJD3 is a histone H3K27 demethylase. Cell Res. 2007;17(10):850–7. [PubMed: 17923864]
25. Hong S, Cho YW, Yu LR, Yu H, Veenstra TD, and Ge K. Identification of JmjC domain-containing UTX and JMJD3 as histone H3 lysine 27 demethylases. Proc Natl Acad Sci U S A. 2007;104(47):18439–44. [PubMed: 18003914]
26. Miller SA, Mohn SE, and Weinmann AS. Jmjd3 and UTX play a demethylase-independent role in chromatin remodeling to regulate T-box family member-dependent gene expression. Mol Cell. 2010;40(4):594–605. [PubMed: 21095589]
27. Salminen A, Kaarniranta K, Hiltunen M, and Kauppinen A. Histone demethylase Jumonji D3 (JMJD3/KDM6B) at the nexus of epigenetic regulation of inflammation and the aging process. *J Mol* Med (Berl). 2014;92(10):1035–43. [PubMed: 24925089]
28. Agger K, Cloos PA, Christensen J, Pasini D, Rose S, Rappsilber J, et al. UTX and JMJD3 are histone H3K27 demethylases involved in HOX gene regulation and development. Nature. 2007;449(7163):731–4. [PubMed: 17713478]
29. Shi J, Wang E, Milazzo JP, Wang Z, Kinney JB, and Vakoc CR. Discovery of cancer drug targets by CRISPR-Cas9 screening of protein domains. Nat Biotechnol. 2015;33(6):661–7. [PubMed: 25961408]

30. Gundry MC, Brunetti L, Lin A, Mayle AE, Kitano A, Wagner D, et al. Highly Efficient Genome Editing of Murine and Human Hematopoietic Progenitor Cells by CRISPR/Cas9. Cell Rep. 2016;17(5):1453–61. [PubMed: 27783956]

31. Kruidenier L, Chung CW, Cheng Z, Liddle J, Che K, Joberty G, et al. A selective jumonji H3K27 demethylase inhibitor modulates the proinflammatory macrophage response. Nature. 2012;488(7411):404–8. [PubMed: 22842901]

32. Weng AP, Ferrando AA, Lee W, Morris JPt, Silverman LB, Sanchez-Irizarry C, et al. Activating mutations of NOTCH1 in human T cell acute lymphoblastic leukemia. Science. 2004;306(5694):269–71. [PubMed: 15472075]

33. Malecki MJ, Sanchez-Irizarry C, Mitchell JL, Histen G, Xu ML, Aster JC, et al. Leukemia-associated mutations within the NOTCH1 heterodimerization domain fall into at least two distinct mechanistic classes. Mol Cell Biol. 2006;26(12):4642–51. [PubMed: 16738328]

34. Thompson BJ, Buonamici S, Sulis ML, Palomero T, Vilimas T, Basso G, et al. The SCFFBW7 ubiquitin ligase complex as a tumor suppressor in T cell leukemia. J Exp Med. 2007;204(8):1825–35. [PubMed: 17646408]

35. O'Neil J, Grim J, Strack P, Rao S, Tibbitts D, Winter C, et al. FBW7 mutations in leukemic cells mediate NOTCH pathway activation and resistance to gamma-secretase inhibitors. J Exp Med. 2007;204(8):1813–24. [PubMed: 17646409]

36. Kourtis N, Lazaris C, Hockemeyer K, Balandran JC, Jimenez AR, Mullenders J, et al. Oncogenic hijacking of the stress response machinery in T cell acute lymphoblastic leukemia. Nat Med. 2018;24(8):1157–66. [PubMed: 30038221]

37. Srivastava S, Sahu U, Zhou Y, Hogan AK, Sathyan KM, Bodner J, et al. NOTCH1-driven UBR7 stimulates nucleotide biosynthesis to promote T cell acute lymphoblastic leukemia. Sci Adv. 2021;7(5).

38. Joshi I, Minter LM, Telfer J, Demarest RM, Capobianco AJ, Aster JC, et al. Notch signaling mediates G1/S cell-cycle progression in T cells via cyclin D3 and its dependent kinases. Blood. 2009;113(8):1689–98. [PubMed: 19001083]

39. Wendorff AA, Quinn SA, Rashkovan M, Madubata CJ, Ambesi-Impiombato A, Litzow MR, et al. Phf6 Loss Enhances HSC Self-Renewal Driving Tumor Initiation and Leukemia Stem Cell Activity in T-ALL. Cancer Discov. 2019;9(3):436–51. [PubMed: 30567843]

40. Figueroa ME, Chen SC, Andersson AK, Phillips LA, Li Y, Sotzen J, et al. Integrated genetic and epigenetic analysis of childhood acute lymphoblastic leukemia. J Clin Invest. 2013;123(7):3099–111. [PubMed: 23921123]

41. Mullighan CG, and Downing JR. Global genomic characterization of acute lymphoblastic leukemia. Semin Hematol. 2009;46(1):3–15. [PubMed: 19100363]

42. Liu Y, Easton J, Shao Y, Maciaszek J, Wang Z, Wilkinson MR, et al. The genomic landscape of pediatric and young adult T-lineage acute lymphoblastic leukemia. Nat Genet. 2017;49(8):1211–8. [PubMed: 28671688]

43. Van der Meulen J, Sanghvi V, Mavrakis K, Durinck K, Fang F, Matthijssens F, et al. The H3K27me3 demethylase UTX is a gender-specific tumor suppressor in T-cell acute lymphoblastic leukemia. Blood. 2015;125(1):13–21. [PubMed: 25320243]

44. Van Vlierberghe P, and Ferrando A. The molecular basis of T cell acute lymphoblastic leukemia. J Clin Invest. 2012;122(10):3398–406. [PubMed: 23023710]

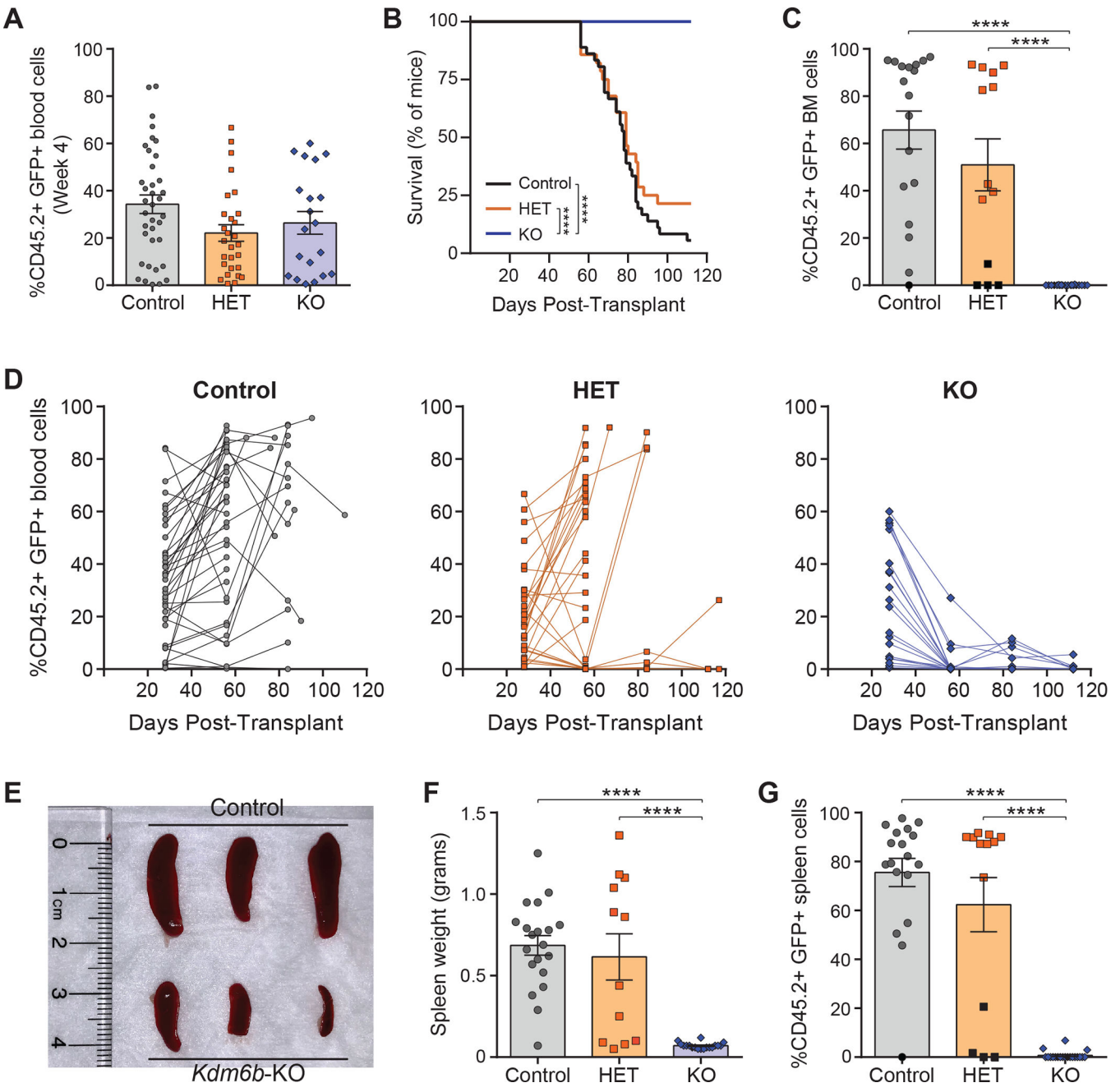

Figure 1: Kdm6b is essential for maintenance of NOTCH1-mutant T-ALL cells

A) T-ALL (CD45.2+ GFP+) engraftment in peripheral blood of mice transplanted with Control (n=37), *Kdm6b*-HET (n=28), and *Kdm6b*-KO (n=20) NICD-expressing cells four-weeks post-transplant.

B) Kaplan-Meier plot of mice transplanted with Control (n=37), *Kdm6b*-HET (n=28), and *Kdm6b*-KO (n=20) NICD-expressing T-ALL cells.

C) T-ALL burden in the bone marrow of moribund mice. Black shapes indicate mice that did not develop disease during the experimental timecourse.

D) T-ALL disease burden in the peripheral blood of individual mice over the experimental timecourse.
E) Representative spleens from mice transplanted with T-ALL cells of indicated genotypes.
F) Spleen weights from moribund mice.
G) T-ALL burden in the spleens of moribund mice. Black shapes indicate mice that did not develop disease during the experimental timecourse.
**** $p<0.0001$. Data analyzed by log-rank Mantel-Cox test (B), or one-way ANOVA with Tukey correction for multiple comparisons (A, C, F, G).

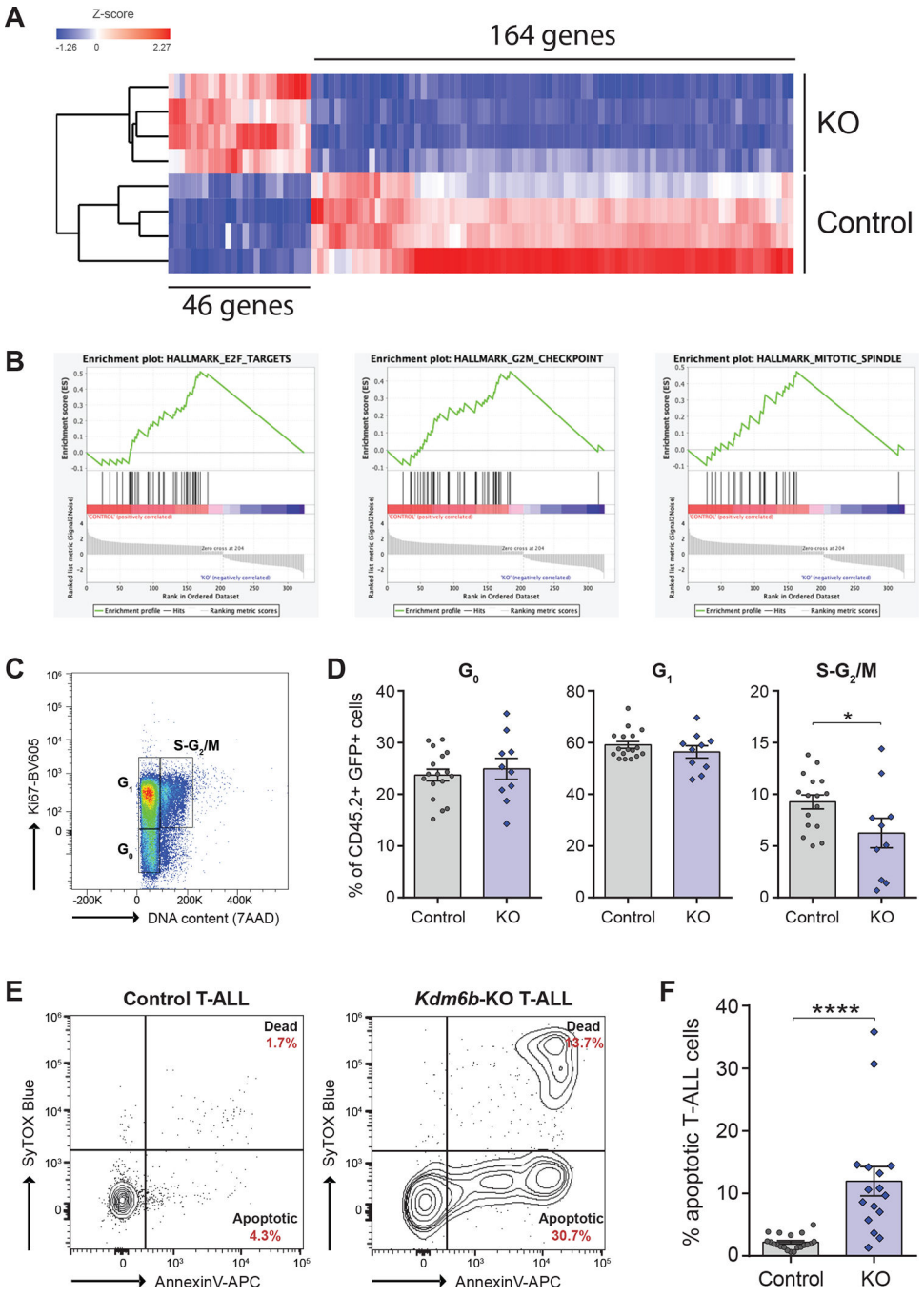

Figure 2: T-ALL cells undergo apoptosis in the absence of Kdm6b

A) Hierarchical clustering of genes with >2-fold expression change (*p*-value <0.05, FDR <0.05) between control and *Kdm6b*-KO T-ALL cells.

B) Gene set enrichment analysis (GSEA) identified three significantly enriched pathways involved in cell cycle regulation downregulated in *Kdm6b*-KO T-ALL cells.

C) Representative flow cytometry plot showing Ki67 cell cycle analysis of T-ALL cells from the peripheral blood of mice.

D) Cell cycle analysis of control and *Kdm6b*-KO T-ALL cells from the blood of recipient mice four-weeks post-transplant.
E) Representative flow cytometry plots showing AnnexinV apoptosis analysis of T-ALL cells from the peripheral blood of mice.
F) Quantification of apoptotic NICD-expressing T-ALL cells from blood of recipient mice four-weeks post-transplant.
* $p<0.05$, **** $p<0.0001$. Data analyzed by two-tailed t-test (D, F).

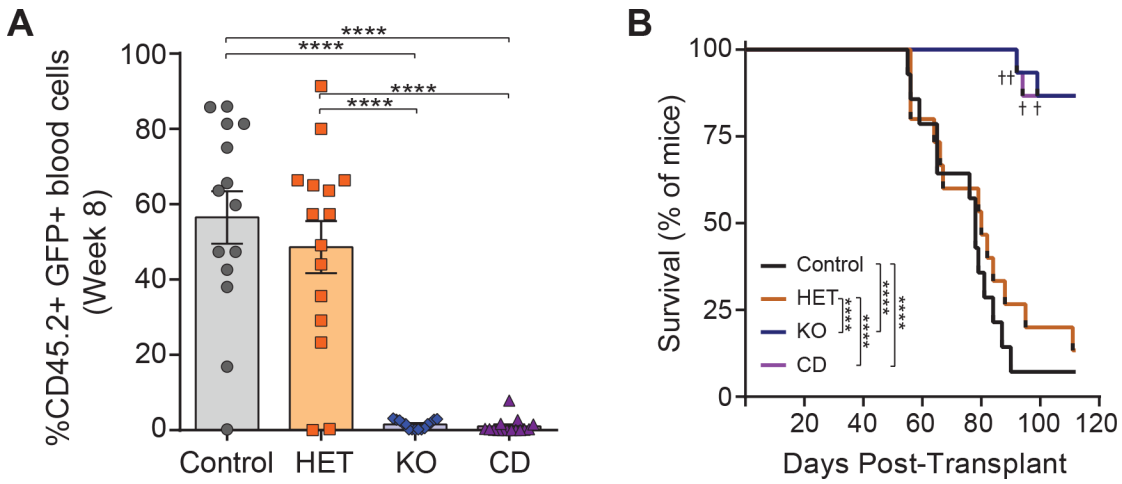

Figure 3: Pro-tumorigenic function of Kdmb6 in T-ALL is demethylase-dependent

A) T-ALL (CD45.2+ GFP+) engraftment in peripheral blood of mice transplanted with Control (n=14), *Kdm6b*-HET (n=15), *Kdm6b*-KO (n=15) and *Kdm6b*-CD (n=15) NICD-expressing cells eight-weeks post-transplant.

B) Kaplan-Meier plot of mice transplanted with Control (n=15), *Kdm6b*-HET (n=15), *Kdm6b*-KO (n=15) and *Kdm6b*-CD (n=15) T-ALL cells.

**** p<0.0001. Data analyzed by one-way ANOVA with Tukey correction for multiple comparisons (A) or log-rank Mantel-Cox test (B).

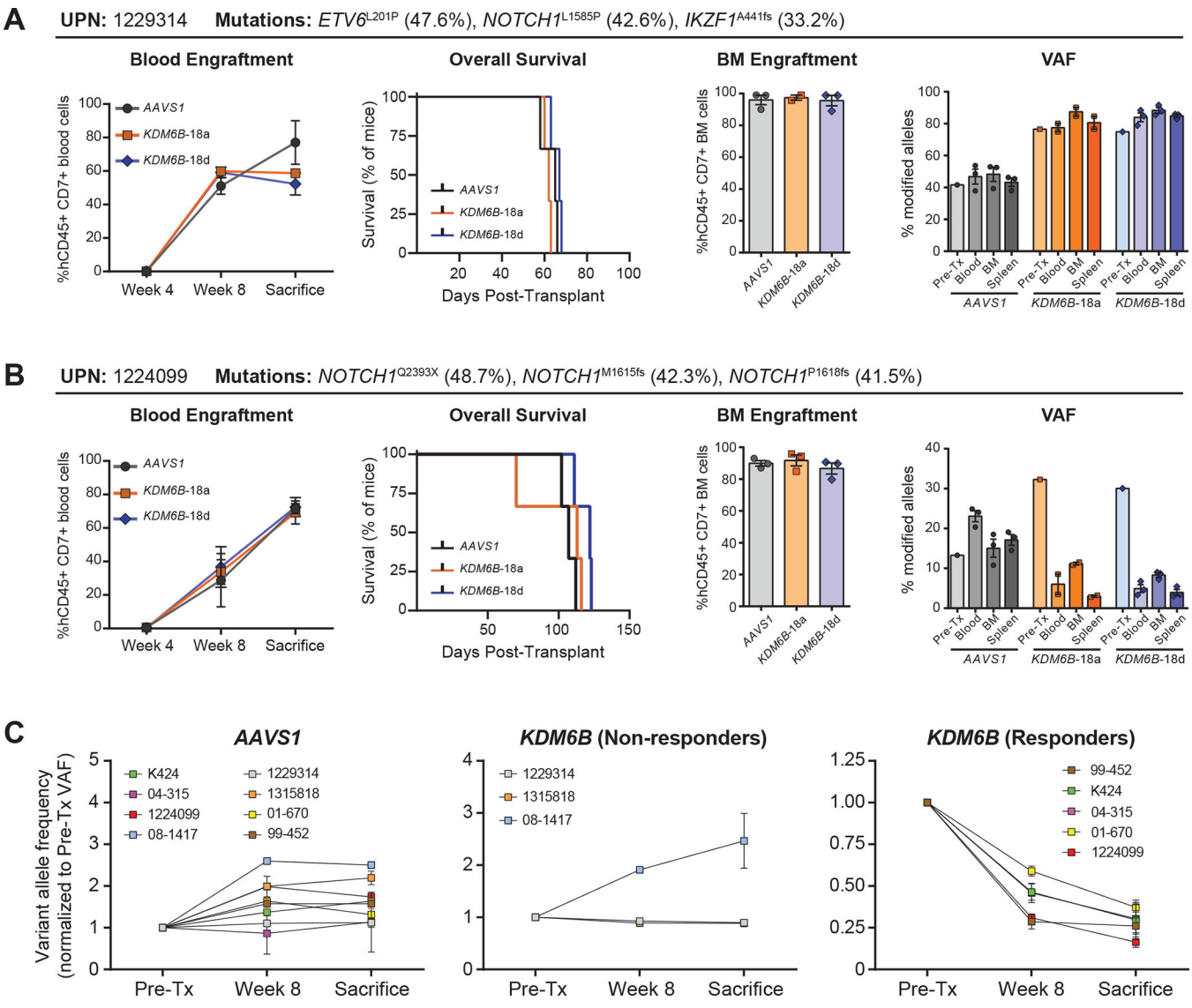

Figure 4: KDM6B is required to sustain disease in a subset of T-ALL patients

A) Patient-derived xenograft of a representative KDM6B "non-responder" adult T-ALL patient sample showing peripheral blood engraftment of human T-ALL cells (hCD45+ hCD7+), overall survival, bone marrow engraftment of T-ALL cells from moribund mice and variant allele frequency of CRISPR edited targets.

B) Patient-derived xenograft of a representative KDM6B "responder" adult T-ALL patient sample showing peripheral blood engraftment of human T-ALL cells (hCD45+ hCD7+), overall survival, bone marrow engraftment of T-ALL cells from moribund mice and variant allele frequency of CRISPR edited targets.

C) Dynamic analysis of CRISPR edits in adult T-ALL cells over the experimental timecourse showing VAF of *AAVS1* control and *KDM6B* segregated into responders versus non-responders. VAF is normalized to the initial CRIPSR efficiency in cells prior to transplant. For *KDM6B* VAF, values represent compiled normalized values for two independent gRNAs per sample.

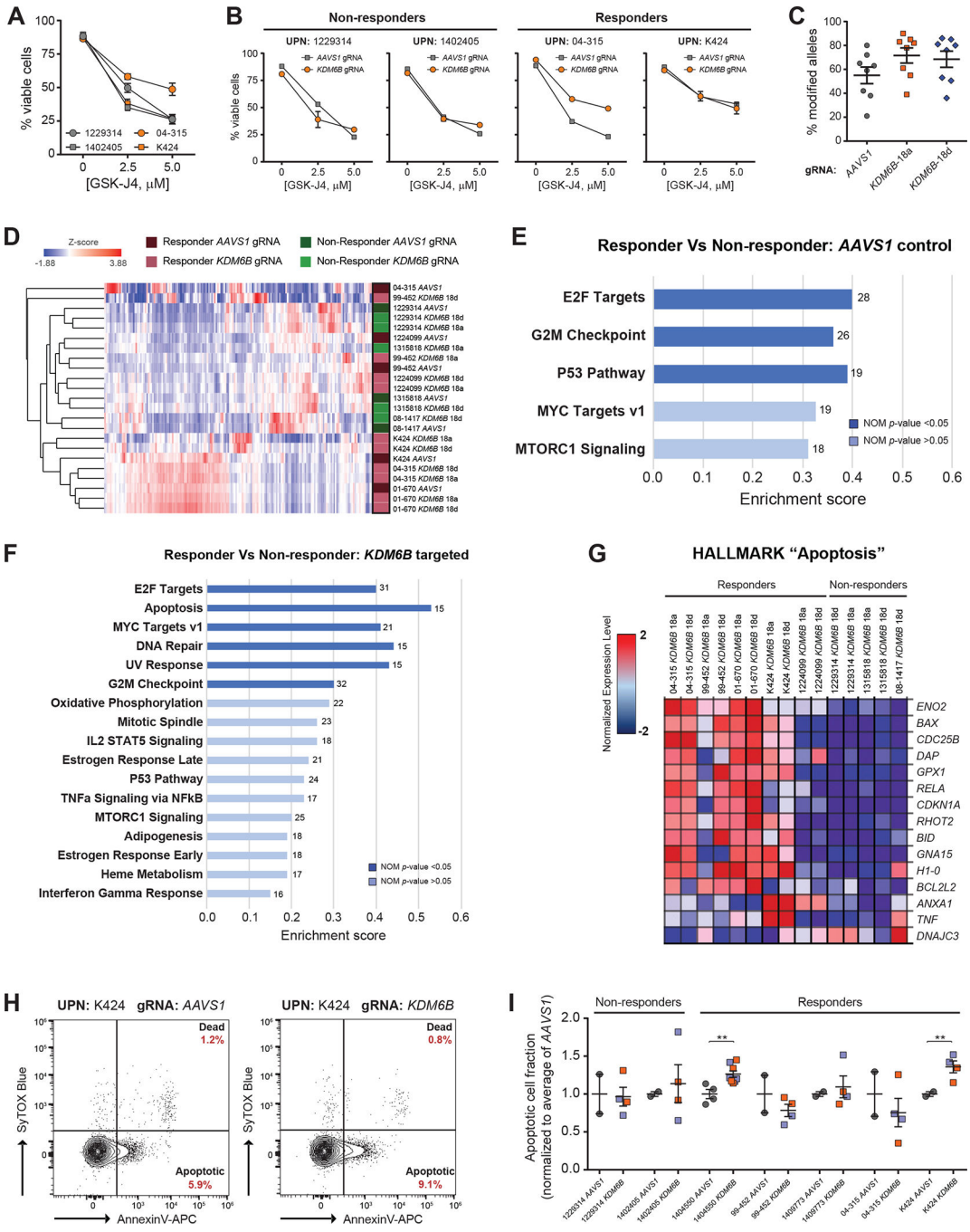

Figure 5: KDM6B restrains expression of pro-apoptotic genes in KDM6B-dependent T-ALLs

A) Cell viability of KDM6B responder (orange) and non-responder (grey) patient samples after 48-hours *in vitro* treatment with increasing concentrations of GSK-J4.

B) Cell viability of T-ALL patient samples following CRISPR editing with indicated gRNAs after 48-hours *in vitro* treatment with increasing concentrations of GSK-J4.

C) VAF of indicated CRISPR edits in primary T-ALL patient cells following seven-days *in vitro* culture.

D) Unsupervised clustering of normalized RNA-seq gene expression data of primary T-ALL patient samples targeted for either *AAVS1* or *KDM6B* by CRISPR gene editing.
E) Gene set enrichment of KDM6B responder versus non-responder samples targeted with *AAVS1* gRNA (control conditions). Numbers atop each bar show number of genes within specified geneset.
F) Gene set enrichment of KDM6B responder versus non-responder samples targeted with *KDM6B* gRNAs. Numbers atop each bar show number of genes within specified geneset.
G) Heatmap of gene expression in HALLMARK "Apoptosis" gene signature that was significantly enriched in responder T-ALL patient samples after targeting with *KDM6B* gRNAs.
H) Representative flow cytometry plots showing AnnexinV apoptosis staining of T-ALL patient sample after CRISPR targeting with indicated gRNAs and seven-days *in vitro* culture. I) Relative fraction of apoptotic cells (normalized to average *AAVS1* AnnexinV+ cells per patient) within T-ALL patient samples after CRISPR targeting with indicated gRNAs and seven-days *in vitro* culture. Orange and blue values for *KDM6B* group indicate two different gRNAs.
** $p<0.01$. Data analyzed by two-tailed t-test relative to the *AAVS1* control for each individual patient (I).

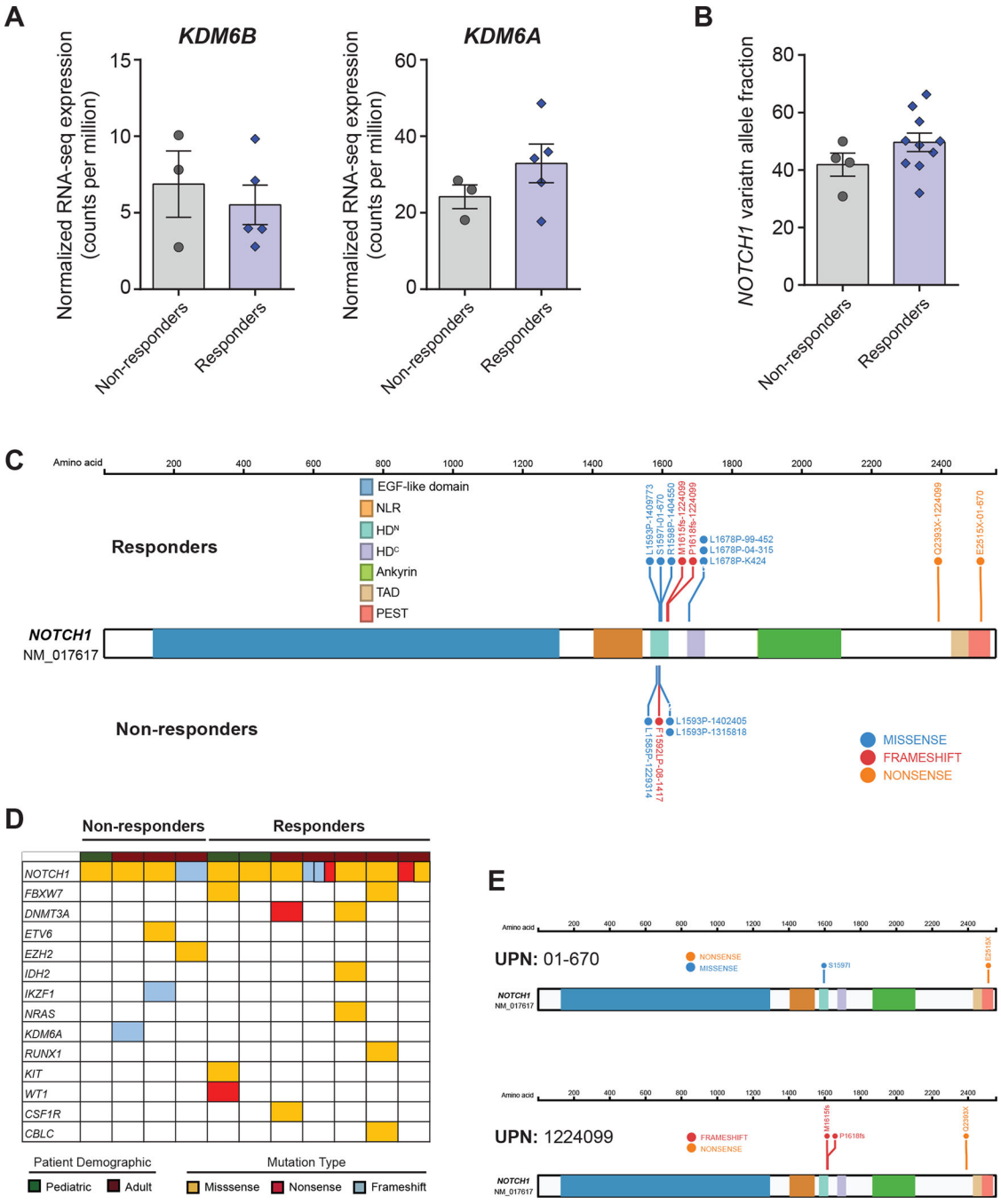

Figure 6: Genetic signature of KDM6B dependence in T-ALL

A) Normalized mRNA expression of *KDM6B* and *KDM6A* in KDM6B responder versus non-responder T-ALL patient samples.

B) Variant allele frequency of *NOTCH1* mutations in KDM6B responder versus non-responder T-ALL patient samples.

C) Distribution of mutations across *NOTCH1* in KDM6B responder versus non-responder T-ALL patient samples.

D) Co-occurrence of genes recurrently mutated in T-ALL in KDM6B responder versus non-responder T-ALL patient samples. Patients with multiple mutations in *NOTCH1* are denoted by multiple boxes within *NOTCH1* column.
E) Distribution of mutations across *NOTCH1* in KDM6B responder patient samples with multiple *NOTCH1* mutations.

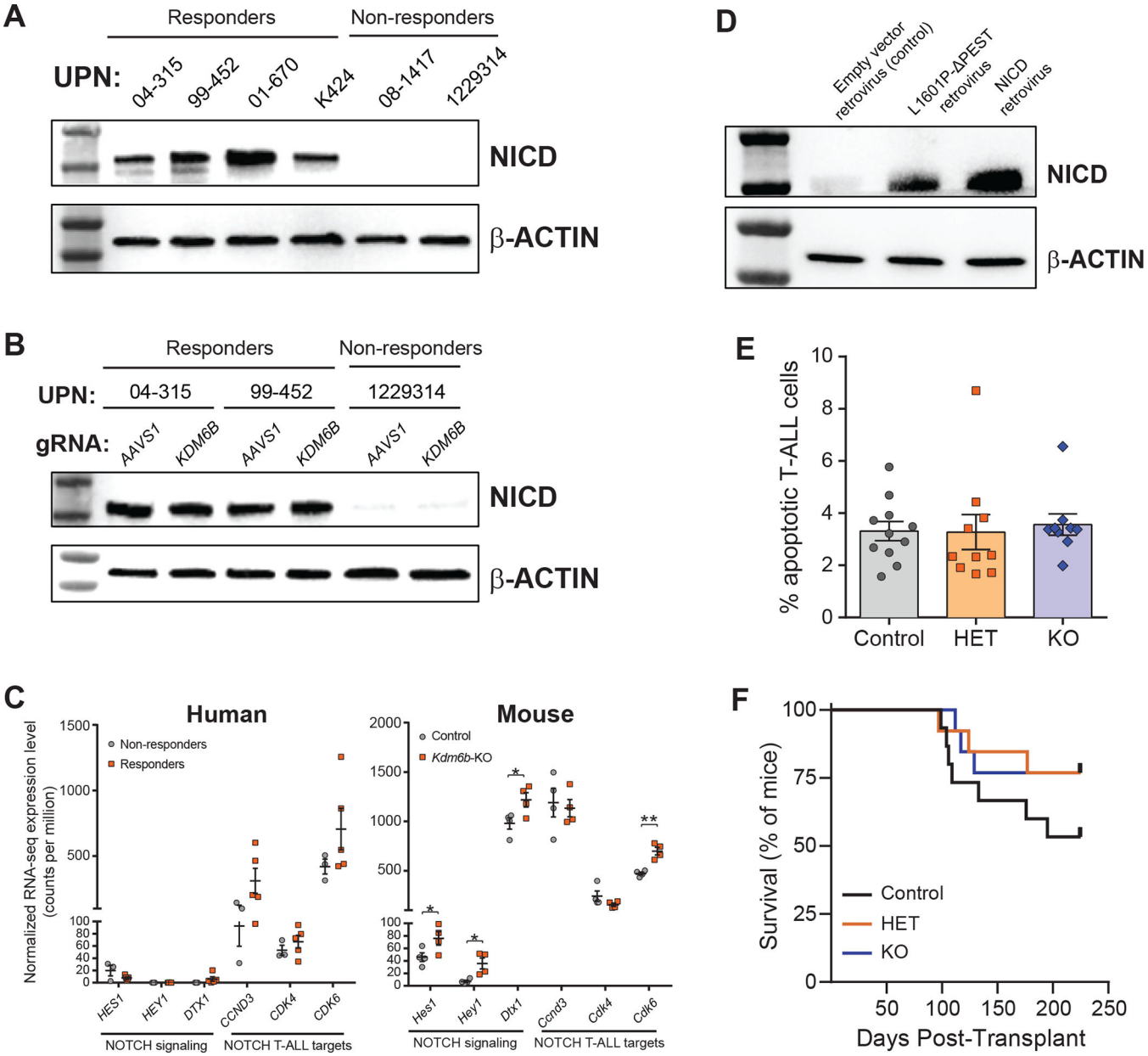

Figure 7: KDM6B protects T-ALL cells from strong NOTCH1 signaling-induced apoptosis

A) Western blot showing protein levels of cleaved NOTCH1 (NICD) in KDM6B responder versus non-responder T-ALL patient samples.

B) Western blot showing protein levels of cleaved NOTCH1 (NICD) in KDM6B responder versus non-responder T-ALL patient samples 48-hours post-targeting with indicated gRNAs.

C) RNA-seq expression levels of classic NOTCH1 signaling genes and NOTCH1 T-ALL target genes in human KDM6B responder versus non-responder T-AL patient samples, and control and *Kdm6b*-KO mouse T-ALL cells.

D) Western blot comparing protein levels of cleaved NOTCH1 (NICD) in cells transduced with indicated *NOTCH1* mutant retroviral constructs compared to the empty vector control.

E) Quantification of apoptotic *NOTCH1*^{L1601P}-ΔPEST-expressing T-ALL cells from blood of recipient mice four-weeks post-transplant.
F) Kaplan-Meier plot of mice transplanted with Control (n=15), *Kdm6b*-HET (n=13), and *Kdm6b*-KO (n=13) *NOTCH1*^{L1601P}-ΔPEST-expressing T-ALL cells.
* p<0.05, ** p<0.01. Data analyzed by two-tailed t-test (C).

Table 1:

T-ALL patient sample characteristics.

Patient ID	Demographic	*NOTCH1* Mutation (VAF)	Other Pathogenic Mutations (VAF)	*KDM6B* Inhibition Status
1315818	Adult	L1593P (49.9%)	*KDM6A*^{V1165fs} (26.9%)	Non-responder
1229314	Adult	L1585P (42.6%)	*ETV6*^{L201P} (47.6%), *IKZF1*^{A441fs} (33.2%)	Non-responder
08–1417	Adult	F1592LP (30.9%)	*EZH2*^{D657Y} (54.2%)	Non-responder
K424	Adult	L1678P (62.2%)	*CSF1R*^{E955K} (53.9%), *DNMT3A*^{R598X} (48.1%)	Responder
1224099	Adult	Q2393X (48.7%), M1615fs (42.3%), P1618fs (41.5%)	N.D.	Responder
04–315	Adult	L1678P (32.0%)	*DNMT3A*^{W860R} (96.3%), *NRAS*^{G12D} (47.1%), *IDH2*^{R140Q} (42.7%),	Responder
99–452	Adult	L1678P (46.1%)	*FBXW7*^{R441Q} (49.1%), *RUNX1*^{L56S} (46.2%), *CBLC*^{P435S} (34.0%)	Responder
01–670	Adult	E2515X (56.8%), S1597I (50.0%)	N.D.	Responder
1402405	Pediatric	L1593P (44.1%)	N.D.	Non-responder
1404550	Pediatric	R1598P (50.2%)	*FBXW7*^{R505C} (51.6%)	Responder
1409773	Pediatric	L1593P (66.2%)	*WT1*^{Q209X} (49.3%), *KIT*^{T274M} (40.5%)	Responder

N.D. = not detected.